HEFAT2007
5th International Conference on Heat Transfer, Fluid Mechanics and Thermodynamics
Sun City, South Africa
Paper number: AT1

CONVECTION HEAT TRANSFER IN BAFFLED MIXING TANK

Tuomo Aho and Reijo Karvinen
Tampere University of Technology
Energy and Process Engineering
P.O.Box 589, FIN-33101 Tampere, Finland
Tuomo.Aho@tut.fi

ABSTRAC

Single -phase flow field and temperature distribution in a baffled tank stirred by a three- bladed impeller was investigated both computationally and experimentally. The computational model employed a sliding mesh technique in fully three-dimensional grids for a small-scale unit, in which also velocity and heat transfer measurements were made with water. Turbulence effects were simulated using the standard k-ε model. Two different boundary conditions, namely, constant heat flux and constant temperature on the wall were used for heat transfer simulations. Mean velocity and turbulence were measured using LDA. In temperature measurements thermocouples were used. By comparing experimental and modelled results non-dimensional variables of velocity were found, which gave very similar results to the pilot unit and full- size reactor of 12 m^3, for which some modelled heat transfer results are given.

NOMENCLATURE

D	[m]	tank diameter
d	[m]	impeller diameter
H	[m]	tank height
k	[m^2/sec^3]	turbulence kinetic energy
LDA		Laser-Doppler anemometry
L_1, L_2, L_3	[m]	baffle distances
N	[rpm]	rotational speed
N_{Re}		impeller Reynolds number
PIV		Particle Image velocimetry
q	[W/m^2]	heat flux
R	[m]	tank radius
R_1, R_2	[m]	bottom radius
R_{bl}	[m]	impeller blade radius
r	[m]	radial coordinate
T	[°]	mean temperature
U	[m/s]	axial mean velocity
W_{tip}	[m/s]	impeller tip speed
W	[m/s]	tangential mean velocity
x	[m/s]	axial coordinate

Special characters

ε	[m^2/sec^3]	turbulence dissipation
μ	[kg/s/m]	dynamic viscosity
ρ	[kg/m3]	density
τ	[sec]	time
ϕ	[°]	tangential coordinate

Superscripts

*	dimensionless parameter

INTRODUCTION

Impeller-stirred reactors are widely used in the chemical industry to provide effective mixing of chemical reactants to form desired products. The type of impeller determines flow patterns and therefore the efficiency of the mixing process. Knowledge of factors such as mixing efficiency, heat transfer rate, residence time and concentration levels are critical to the successful operation of an impeller-stirred tank. These key operating factors are typically investigated by conducting measurements using a small pilot- or bench-scale equipment. Accurate measurements in commercial scale units are difficult and often impossible to carry out. The smaller scale testing process is usually scaled up to commercial scale operating conditions. Since the scaling procedure is also very complex, scale-up models for mixing tanks have been limited. Computational fluid dynamics provides a useful method to simulate the performance of both bench-scale and full-size units. Much work on stirred tank computations in three dimensions has been carried out in the last few years using different types of methods. In the first stage, the impeller was replaced by a jet and turbulence was handled with the two-equation models of turbulence [1]. Later on, also the impeller could be included in predictions employing a rotation mesh around the impeller [2]. In order to couple together the impeller and the remainder of the tank there are many possibilities: steady- state, quasi-static and transient approaches [3]. As a matter of fact, the methods are same as in the modelling of impeller pumps [4]. If use is made of two-equation models details of turbulence cannot be found. If extended computational resources are available, more sophisticated approaches like LES can be adopted [5]. There also exist plenty of experimental papers in the literature. Mean velocities [6] and power consumption have been measured [7] and dimensionleess numbers have been tried to found to descript the performance [8]. During recent years the structure of turbulence in a mixing tank has also been measured with PIV and LDA [9,10].

Published data for the case of a stirred tank with heat transfer are very limited and there exist only some papers [11]. The objective of this investigation is to model the velocity field, to map the temperature

distributions and to model heat transfer in a stirred tank. To obtain this goal, an impeller-stirred tank is modeled using computational fluid dynamics simulations with a sliding grid technique, which has been applied successfully for the stirred tanks in earlier studies [2,3,12]. Simulations are carried out with two different boundary conditions for heat transfer. Data from LDA measurements of mean velocities in a bench-scale unit are used to validate calculated velocities. Measurements of actual temperature distribution are provided as a basis for checking model reliability.

STIRRED VESSEL CONFIGURATION

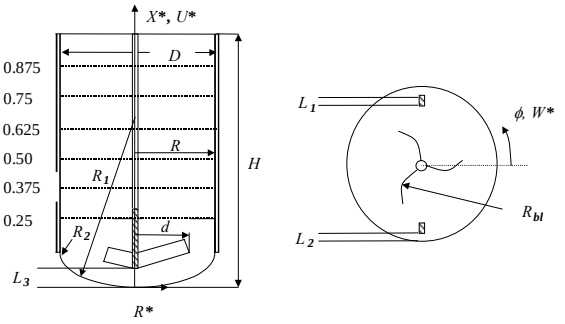

Figure 1 Gross-section and plan view of bench-scale stirred tank and blade impeller.

Figure 1 shows a schematic diagram of the experimental stirred tank and blade impeller. The cylindrical tank with an inner diameter D of 246 mm was filled with water at room temperature to a height of 329 mm from tank bottom. The mixing vessel had a dished bottom,the curvature of which is given by R_1 and R_2 equal to 197 mm and 38 mm, respectively. The tank was equipped with two internal baffles each with a width L_1 of 18.5 mm. Both baffles were mounted at a distance L_2 of 18.5 mm (0.075D) from the tank wall. The clearance between each baffle and the tank bottom L_3 was 61.5 mm. The curved blade impeller diameter d and width were 138 mm and 25 mm, respectively. The radius of the blade curvature, R_{bl}, was 61.5 mm, and the blades were tilted 10 degrees past vertical (-10 degrees rake).

NUMERICAL MODELLING

The sliding grid method was used for three-dimensional flow velocity field modeling around the complex impeller . Turbulence was modeled using the standard k-ε model in conjunction with logarithmic wall functions. The commercially available computational package CFX was used in modelling. At the beginning of the calculation, a time-step size was chosen such that a rotation of the inner grid zone was one half the angle increment between the impeller blades, i.e. 60°. The final steady-cyclic operating conditions were then achieved by starting from the calculated velocity field as an initial condition and then choosing a time-step so that the grid rotates through one azimuthal cell at the each time step.

The calculations were performed using a non-uniform multiblock grid generation technique. Four grid densities were used for checking the solution dependency on the grid density. Especially, at the near wall region, where heat transfer takes place, the grid density must be large. The fine grid consisted of 115200 cells. The surface grid for the coarse case and a side cross-section for the fine grid are illustrated in Figure 2. The solved velocity field was used for heat transfer calculations as an initial guess. The fluid was water, for which density and specific heat can be assumed constant, but the effect of temperature on viscosity was taken into acconunt. The no-slip condition is applied at the surface of the vessel, baffles, impeller blades and shaft. The free surface is treated as a plane of symmetry. Heat flux through the free surface and tank bottom was assumed to be zero.

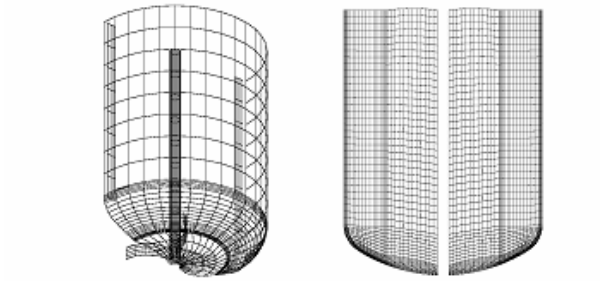

Figure 2 Coarse surface grid and side cross-section for fine grid.

EXPERIMENTAL TECHNIQUES

Velocity Measurements

Laser-Doppler anemometry (LDA) system is shown in Figure 3. The vessel was placed in a square plexiglass tank filled with water in order to minimize laser beam refraction through the curved tranparent plastic surface of the cylindrical mixing vessel. The tank bottom was manufactured from opaque, white plastic which extended to a height of 60 mm from the tank bottom surface. This opaque region could not be penetrated by the laser beam, so measurements and data collection in this region was not possible. A transparent acrylic lid was fitted on the top of the mixing tank at height H to prevent the entrainment of air bubbles from the free surface into the flow.

An Ar-ion laser generated a multicolour laser beam, which was then split into two green and two blue beams in a transmitter. These beams were transferred through fiber optical cables to transmitting and receiving optics, which converged the beams to intersect and form a small elliptical control volume. Water in the stirred tank was seeded with titanium oxide particles of an approximately mean diameter of 10 μm, which scattered light as they travelled through the control volume. The scattered laser light was then collected by receiving optics and the resulting Doppler shift was measured with photodetectors. A signal processor converted electric signals from the photodetectors into

digital information for computer processing. On the computer, measurements were used to produce both average and fluctuating velocities on-line.

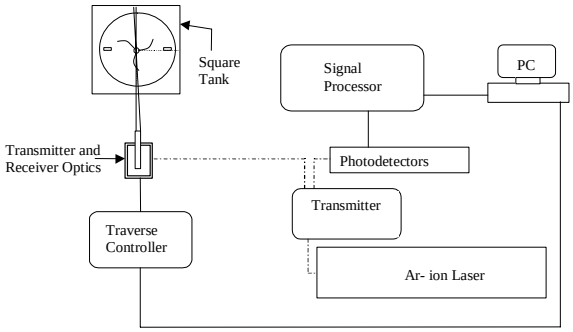

Figure 3 Laser-Doppler velocimetry system.

The computer-driven traverse controller was used to move the laser probe in a predetermined grid. Data for axial and tangential velocity components were measured at one vertical plane, ie. $\phi = 0°$. A grid with six different axial heights in Figure 1(X^* equal to 0.25, 0.375, 0.50, 0.625, 0.75 and 0.875) and 36 radial measuring points at each height was set up to obtain a total of 216 measuring locations in the tank. Due to the shaft symmetry, only one half of the tank was mapped.

Since there were two pairs of laser beams and the traverse controller could move in two directions, it was possible to measure two velocity components simultaneously. The axial and tangential velocity components were chosen for measurement, since the radial velocity component is insignificant in the region adjacent to wall where heat transfer takes place. The criterion for the duration of data acquisition was set at 10 000 validated samples or 3 minutes time period. However, at the bottom part of the tank, there was distinct discrepancy between the measured and calculated tangential velocities in region near the wall. Due to this discrepancy, the velocity measurements were repeated at the three lowest measuring heights. The new criterion for data acquisition duration was increased to 20 000 validated samples or a 5 minutes time period.

The impeller Reynolds number N_{Re} based on rotational speed N_s and diameter d is defined as:

$$N_{\mathrm{Re}} = \frac{\rho N_s d^2}{\mu}$$

Three measured rotation speeds with respective impeller tip speeds and Reynolds numbers are given in Table 1. More details can be found in reference [13].

Table 1 Measured rotation speeds.

Experiment	N_s (r/s)	N_{Re}	W_{tip} (m/s)
expt1	6.52	$1.23*10^4$	2.83
expt2	9.75	$1.85*10^4$	4.23
expt3	11.38	$2.16*10^4$	4.94

Heat Transfer Experiments

The apparatus shown in Figure 4 was used to experimentally obtain the temperature field in the stirred tank filled with water in a a room temperature. The geometry of the tank was the same as in velocity experiments. However, in order to make wall heat transfer resistance negligible, copper instead of plastic was used as the wall material of the cylindrical tank. The dished bottom, similar to the one used in the flow measurements, was thermally insulated. A cylindrical heating element encircled the copper wall and provided a constant heat flux of 5000 W/m^2. The outer surface of heating element was insulated to minimize ambient heat loss.

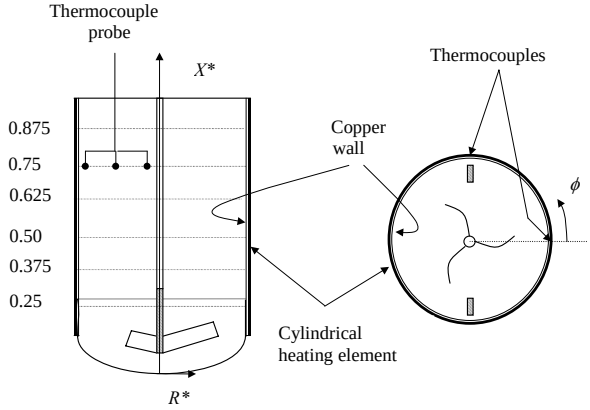

Figure 4 Schematic diagram of heat transfer measurement.

To measure temperature distribution on the wall surface, six copper-constant thermocouples of 0.3 mm in diameter were affixed to the wall with a 41 mm spacing between the heating element and the copper wall at two tangential measuring locations, namely $\phi = 0°$ and $\phi = 90°$ (refer to Figure 4). The temperature field inside in the tank was measured using a probe composed of three thermocouples spaced 40 mm apart from each other. Fluid temperature measurements with the probe were repeated at six different axial heights (X^* equal to 0.25, 0.375, 0.50, 0.625, 0.75 and 0.875, as shown in Figure 4).

RESULTS AND DISCUSSION

Velocity Field

The number of nodes was increased as computation progresses to check that calculated results did not change too much with different grid sizes. The grid refinement testing was carried out using four non-uniform grid systems as mentioned ealier. The test showed that the axial velocity is insensitive to the grid size, the greatest changes in axial velocity occurring near the impeller shaft. Since heat transfer from the wall is considered, the most important velocity components are the axial and tangential components, while the radial velocity component clearly becomes zero at the wall. When comparing the predictions made

with the different meshes, very similar qualitative trends, especially in the near wall area, were obtained.

Figure 5 and 6 show quantitative comparisons of the measured data and predicted normalized axial and tangential mean velocity profiles at some axial heights between two baffles using dimensionless presentation

$$X^* = \frac{x}{H},\quad R^* = \frac{r}{R}, U^* = \frac{U}{W_{tip}}, W^* = \frac{W}{W_{tip}}, k^* = \frac{k}{0.5W_{tip}^2}$$

It can be observed that the predicted velocities show good agreement with the LDA data. In the measured apparatus, there was a lid at a height *H*. However, during simulations, the symmetry boundary condition was used to model the free surface. The lid decreases the velocity near the wall at the upper part of the tank. In addition, a hole in the lid at tank centerline caused a downward flow jet. It can be concluded that the comparison between experimental data and numerical predictions match both quantitatively very well. Thus, the computation gives a sound velocity field prediction.

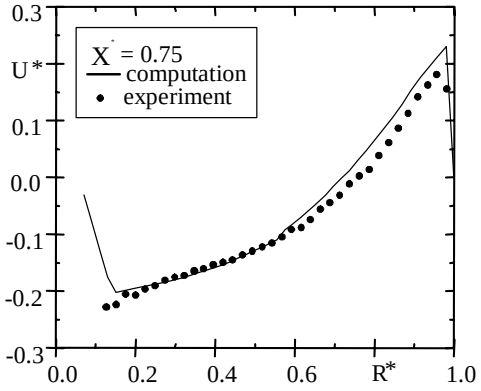

Figure 5 Comparison of computed and measured axial velocities at the high $X^* = 0.75$ ($\phi = 0°$).

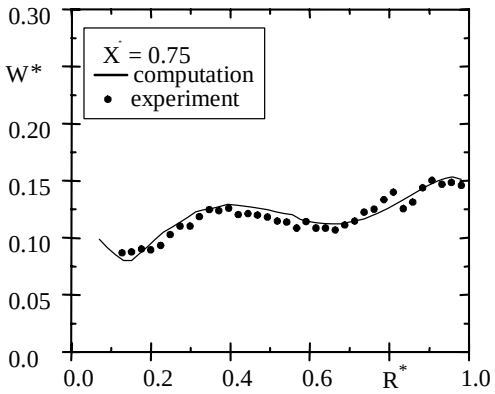

Figure 6 Comparison of computed and measured tangential velocities at the high $X^* = 0.75$ ($\phi = 0°$).

The experimentally determined axial and tangential velocities at three rotation speeds and the predicted profiles for the small-scale and commercial size-unit are reported in Figure 7. These profiles at the bottom part of the tank prove that, if the results are scaled using the chosen dimensionless variables, they could be applied to any rotation speed and any size of the tank. The axial velocity profiles in Figure 7 agree well with each other. The comparison of tangential velocities shows quantitatively similar trends although some differences exist. The reason for differences in tangential velocity component profiles is due to the measuring method. The LDA measurements are more sensitive to disturbances in this case as rotation speed is increased. It was found that the flow is characterized by one large top-to-bottom main circulation loop in both vertical planes. Furthermore, it was noticed that the center of the vertical loop lies close to the wall at the bottom part of the tank. The flow patterns are dominated by the axial velocity component due to the shape of the impeller and the tank bottom, with a strong axial jet flowing upwards at the near wall region and downwards near the shaft. However, at the top of the tank, there is a zone that is nearly stagnant at the top of the tank when examining velocities in the cross-sectional planes.

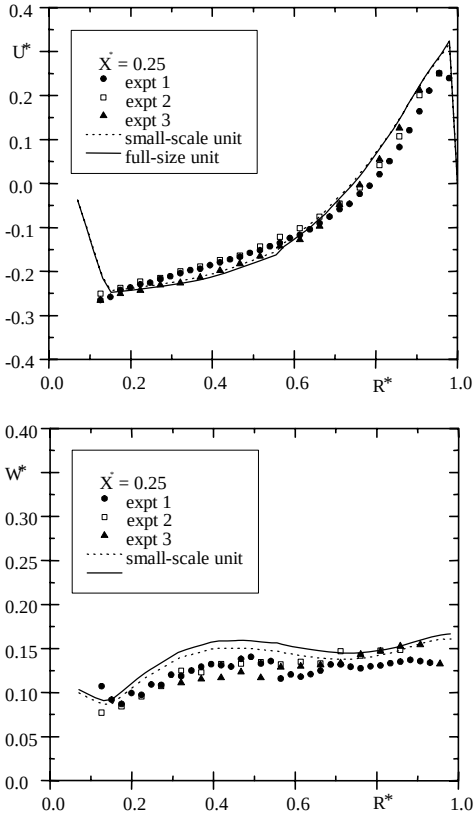

Figure 7 Comparison of small and full size computed axial and tangential velocity profiles to the three measured data at the high $X^* = 0.25$ ($\phi = 0°$).

At the different heights, the maximum axial velocity components upwards and downwards have about the same values. The axial velocity profile shows that the flow direction is upwards, when R^* is between 0.8 and 1.0, but downwards otherwise. The radial component was about one-tenth in magnitude when compared to the axial and tangential components. Axial and tangential components approximately equal in magnitude and dominate the velocity field. The axial

velocity component dominates at the tank bottom and naturally decreases with increasing tank height. At the top part of the tank, the tangential velocity becomes more significant. Figure 6 shows the effect of baffles on the tangential velocity components between the baffles. The presence of a baffle is seen to cause a decrease in tangential velocity in the region behind the baffles between baffle and wall. This can be clearly seen between the baffles especially at the tank top, where the axial velocity component is quite small compared to tangential velocity. The profiles in Figure 6 showed that the actual tangential velocity is highest in a region halfway up the tank.

Heat Transfer

Figure 8 shows the measured wall temperature profiles at 200 seconds time intervals. The predicted wall temperature field after 1000 seconds heating time is also given in Figure 8. It corresponds to the thick profile line on the graph. Figure 8 shows a clearly defined temperature distribution in the axial direction. At the tank bottom, the axial and tangential velocities are highest, therefore the rate of heat transfer is highest, resulting in lowest wall temperatures in this region. The lowest heat transfer coefficient observed was at the top of the tank between the baffles, where there is a relatively stagnant area in the velocity field. Measurements and calculations also showed that there was a temperature difference between tangential locations, thus the heat transfer coefficients vary with angular position with respect to baffle location and the wall temperatures were 2-3 degrees higher between the baffles than near the baffle location. The wall temperatures were lower at the baffle location since flow velocity was highest there, resulting in a higher convective heat transfer rate.

Figure 9 shows a typical predicted temperature field contour on a vertical plane slice located midway between the two internal tank baffles, i.e. ϕ = 0°, for the constant heat flux boundary condition at heating time equal to 1200 seconds. Figure 9 shows how uniform the temperature field is with a constant heat flux boundary condition. The temperature profile develops quickly very near the hot wall, while elsewhere there is adequate mixing to keep the temperature of liquid almost uniform and it varies only by a few degrees in the tank interior. However, the temperature variation along the wall in the axial direction can be found in this countour also.

The average temperature of the fluid as a function of time is illustrated in Figure 9. The fluid temperature was measured with an instrument made up of three thermocouples, which gaged the same temperatures at each of three radial distances. The uniform average temperature variated linearly with respect to time and the measured values were the same as derived from heat balance. The comparison of predicted and measured average liquid temperature predictions agree well, given confidence to predicted results when using the constant wall temperatures as well.

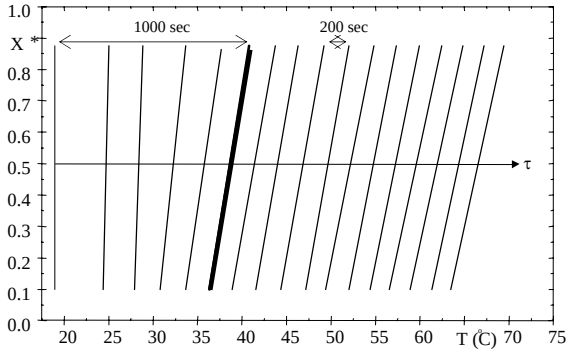

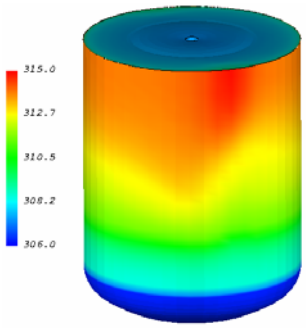

Figure 8. The axial wall temperature profiles at 200 sec time intervals (ϕ = 90°) and predicted wall temperature field after 1000 sec heating.

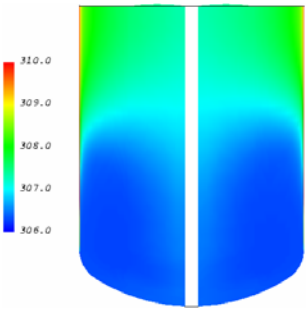

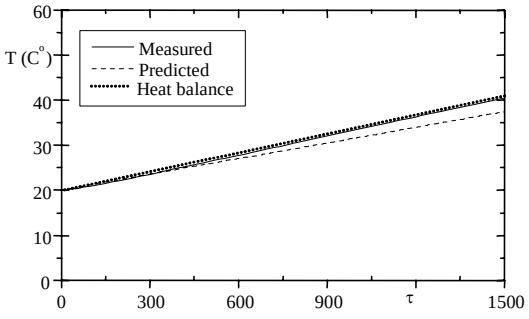

Figure 9 Contour of temperature between two baffles (ϕ = 0° and τ = 1200 sec) on the top. Measured, predicted and heat balance average temperature as function of time, when heat flux on wall is constant.

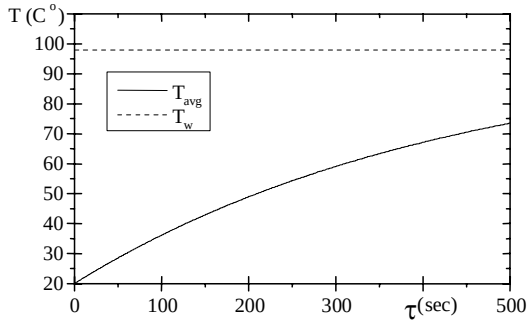

Figure 10 Predicted average temperature as function of time, when T_w = constant in commercial size reactor.

After scaling up the model to the commercial size unit, the constant wall temperature boundary condition was used to model the heat transfer in a commercial unit, which volume was 12 m^3. Figure 10 shows the development of computed mean temperature for a constant wall temperature boundary condition.

CONCLUSIONS

In the study, the numerical predictions of the flow field and temperature distribution of a baffled stirred tank are presented. Grid dependency test showed that the tangential and radial velocities are more sensitive to grid size than the axial component. The results indicate that the flow was dominated by the axial velocity component, resulting in a major top-to-bottom recirculation loop inside the tank. Uniform wall heating boundary condition showed that the wall temperature and the local heat transfer coefficient strongly depended on location. However, the temperature distribution of the liquid was almost uniform and the average temperature of the liquid varied linearly with respect to time. The fluid temperature distribution was clearly defined in the case of an isothermal wall boundary condition. The liquid was warmest at the upper part of the tank and a warm core flowed downwards near the shaft. The variation of the average liquid temperature as a function of time was exponential. In general, the experimental data and the model predictions agree very well. The present study has shown that computational prediction of good accuracy can be obtained across the flow field and temperature distribution in a stirred tank. Thus, a quick assessment of the influence of rotation speed and geometrical variables, such as other types of impellers, can be further explored using only numerical simulations. It is important to note that the two-equation model of turbulence is enough for the modelling of velocity field and heat transfer.

Since the need for more accurate boundary conditions on the jacket side is important, the modelling of the jacket should be scrutinized in future work. Future work should also be directed towards obtaining a detailed technique for rapid heat transfer measurements. A local Nusselt number correlation for a stirred tank as a function of the Reynolds and Prandtl number should be the ultimate goal.

AKNOWLEDGEMENT

The authors gratefully acknowledge the support of Kemira Fine Chemicals Oy and discussions with Dr. P. Oinas.

REFERENCES

[1] Kresta, S.M. and.Wood, P.E.,Prediction of the Three-Dimensional Turbulent Flow in Stirred Tanks, AIChE J.1991;37:448-460.

[2] Ng K., Fentiman N., Lee K. and Yianneskis M., Assessment of Sliding Mesh CFD Predictions and LDA Measurements of the Flow in a Tank Stirred by a Rushton Impeller. Trans IChemE. 1998; 76:737-747.

[3] Micale.G., Brucato,A., and Grsafi,F.,Prediction of Flow Fields in a Dual-Impeller Stirred Vessel.AIChE J. 1999,.45:445-464.

[4] Koivikko, M., Modelling the Effect of Geometric Parameters on the Performance and Efficiency of Centrifugal Pump Impellers, PhD Thesis. Tampere University of Technology, Tampere 2006.

[5] Derksen,J., and Van den Akker,H.E.A., Large Eddy Simulations on the Flow Driven by a Ruston Turbine. AIChE J. 1999;45:209-221.

[6] Komori, S.,and Murakami, Y., Turbulent Mixing in Baffled Stirred Tanks with Vertical-Blate Impellers. AIChE J.1988;34:932-937.

[7] King, R.L., Hiller, R.A. and Taterson, G.B., Power Consumption in a Mixer. AIChE J.1988;34:506-509.

[8] Delaplace,G., guern, R., and Leuliet, J.C., Dimensional Analysis for Planetary Mixer: Modified Power and Reynolds Number.AIChE J.2005;51:3094-3100.

[9] Ducci, A., and Yianneskis, M., Direct Determination of Energy Dissipation in Stirred Vessels with Two-Point LDA. AIChE J.2005;51:2133-2149.

[10] Kilander,J., and Rasmuson, A., Energy Dissipation and Instabilities in a Stirred square tank Investigated Using an LEPIV Approach and LDA measurements.Chemical Engineering Science.2005;60:6844-6856.

[11] Haam, S., Brodkey, R. and Fasano, J., Local Heat Transfer in a Mixing Vessel Using Heat Flux Sensors. Ind. Eng. Chem. Res., Vol. 31, No. 5, 1992, 1384-1391.

[12] Harvey III, A., Lee, C., and Rogers, S., Steady-State Modeling and Experimental Measurement of a Baffled Impeller Stirred Tank, AIChE journal, Vol. 41, No. 10, October 1995, 2177-218.

[13] Aho, T., Fluid Dynamics and Heat Tranfer in a Impeller-Stirred Tank, M.Sc Thesis Tampere University of Technology. Tampere 1999.